JGR Space Physics

RESEARCH ARTICLE
10.1029/2023JA032008

Key Points:

- Citizen scientist photographs revealed fine-scale structures of Strong Thermal Emission Velocity Enhancement
- The fine-scale structures extend down to a 9 km size, possibly even below a 1 km size. They propagate at 8.9 km/s westward
- The power law spectrum with a slope of −1 suggests a shear flow turbulence by the intense subauroral ion drifts

Supporting Information:

Supporting Information may be found in the online version of this article.

Correspondence to:

Y. Nishimura,
toshi16@bu.edu

Citation:

Nishimura, Y., Dyer, A., Donovan, E. F., & Angelopoulos, V. (2023). Fine-scale structures of STEVE revealed by 4K imaging. *Journal of Geophysical Research: Space Physics*, *128*, e2023JA032008. https://doi.org/10.1029/2023JA032008

Received 29 AUG 2023
Accepted 16 NOV 2023

Fine-Scale Structures of STEVE Revealed by 4K Imaging

Y. Nishimura[1], A. Dyer[2], E. F. Donovan[3], and V. Angelopoulos[4]

[1]Department of Electrical and Computer Engineering and Center for Space Physics, Boston University, Boston, MA, USA, [2]AmazingSky Photography, Strathmore, AB, Canada, [3]Department of Physics and Astronomy, University of Calgary, Calgary, AB, Canada, [4]Department of Earth, Planetary, and Space Sciences, University of California, Los Angeles, Los Angeles, CA, USA

Abstract We utilized a 4K imaging to examine properties of fine-scale structures of Strong Thermal Emission Velocity Enhancement (STEVE) near the magnetic zenith. Its high spatial (0.09 km at 200 km altitude) and temporal (24 Hz) resolution provided unprecedented details of fine-scale structures in the subauroral ionosphere. Although the STEVE emission was seen as a homogeneous purple/mauve arc in the all-sky images, the high-speed imaging revealed that STEVE contained substantial multi-scale structures. The characteristic wavelength and period were 12.4 ± 7.4 km and 1.4 ± 0.8 s, and they drifted westward at 8.9 ± 0.7 km/s. The speed is comparable to the reported magnitude of the intense subauroral ion drifts (SAID), suggesting that the fine-scale structures are an optical manifestation of the $E \times B$ drift in the intense SAID. A spectral analysis identified multiple peaks at >10, 4, 2, 1.1, and <1/5 s period (>83, 33, 16, 9, and <1.7 km wavelength). Although most of the fine-scale structures were stable during the drift across the field of view, some of the structures dynamically evolved within a few tens of km. The fine-scale structures have a power law spectrum with a slope of −1, indicating that shear flow turbulence cascade structures to smaller scales. The fine-scale structures pose a challenge to the subauroral ionosphere-thermosphere interaction about how the ionosphere creates such fine-scale structures and how the thermosphere reacts much faster than expected from a typical chemical reaction time.

Plain Language Summary Strong Thermal Emission Velocity Enhancement (STEVE) is often perceived as a homogeneous arc with a purple or mauve color. However, this notion is based on photographs with a long exposure time. We conducted a 4K video observation of STEVE with unprecedentedly high spatial and temporal resolution. The video revealed that STEVE is not a homogeneous arc but consists of rich fine-scale structures that could not be seen in regular photographs. The fine-scale structures had wavelengths of 1–10 s of km with multiple spectral peaks. The fine-scale structures moved westward at 8.9 km/s. We suggest that the fine-scale structures of STEVE correspond to fine-scale plasma structures in the fast plasma streams in the upper atmosphere. However, it is challenging to explain how the upper atmospheric glow can form the fine-scale structure because of the long chemical reaction time.

1. Introduction

Strong Thermal Emission Velocity Enhancement (STEVE) is a purple/mauve arc that appears in the subauroral ionosphere during substorms. It was originally recognized as a homogeneous arc (Størmer, 1935) like a comet tail (Wilson, 1891), and recent photographs support this perception (Archer et al., 2019; Martinis et al., 2022; Parnikov et al., 2022). On the other hand, STEVE was also seen to have fine-scale structures (intensity modulations) along the arc (MacDonald et al., 2018; Mende et al., 2019; Nishimura et al., 2019). The fine-scale structures have a wavelength of few hundred km and drift westward at ∼5–10 km/s (Gillies et al., 2020). The fine-scale structures also evolve over time. STEVE could initially be a homogeneous arc and then develop wave-like fine-scale structures whose wavelengths become shorter in time (Nishimura et al., 2023). This time sequence suggests dynamic evolution of instability along the arc.

Determination of the elementary structures of STEVE is an important issue for understanding the generation mechanism of STEVE. If STEVE is a homogeneous arc, longitudinal dependence is not important for generation of STEVE. But if STEVE consists of fine-scale structures, it becomes a challenge to explain how the ionosphere-thermosphere system creates localized and fast-varying structures. Fine-scale structures could also provide a clue about instabilities that occur in the subauroral ionosphere. Photographs of STEVE often have a

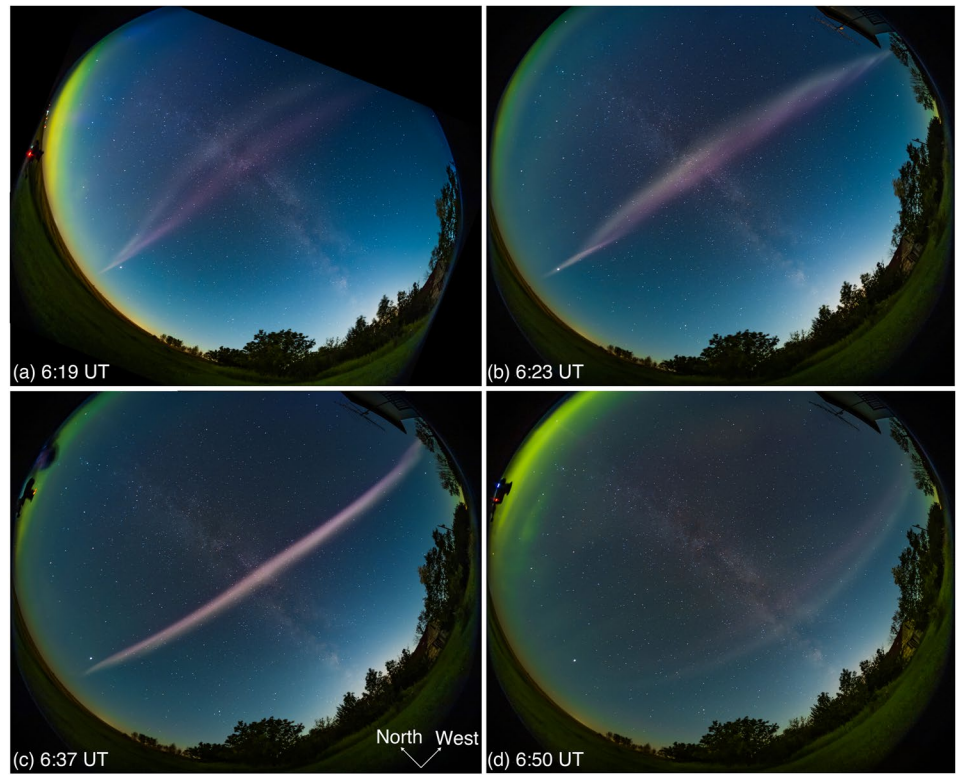

Figure 1. All-sky photographs taken at Strathmore, Canada (58.2° MLAT and 22.2 hr MLT at 06:37 UT) during the Strong Thermal Emission Velocity Enhancement (STEVE) on 8 August 2022. North is to the top left and west is to the top right. The east-west oriented purple/mauve arc is STEVE. The green emission to the north is diffuse aurora in the auroral oval. The exposure time is 20 s.

long (~10 s) exposure time and fine-scale structures are likely smeared out. High-speed imaging is required to determine the elementary structures of STEVE.

A 4K video (3,840 × 2,160 pixels and 24 Hz sampling rate) was taken during STEVE in the night of 8 August 2022. It provided a unique opportunity to examine fine-scale structures of STEVE at much higher resolution than possible in the past. By taking advantage of this observation, we examined properties (velocity, wavelength and period) of the fine-scale structures. We also investigated the frequency spectrum of the fine-scale structures. Data from the citizen scientist photographs, Time History of Events and Macroscale Interactions during Substorms (THEMIS) all-sky imager, spectrograph, and Defense Meteorological Satellite Program (DMSP) were also used to identify the geomagnetic conditions of this event. A potential generation mechanism and open questions were discussed.

2. Results

2.1. The STEVE Event and Geomagnetic Conditions

Figure 1 shows all-sky photographs that were taken at Strathmore, Canada in the night of 8 August 2022. The east-west oriented purple/mauve arc is the STEVE emission of interest. It was located equatorward of the green diffuse emission in auroral oval. It had a characteristic two-band structure (Figure 1a), where the higher-elevation arc contained more enhancements in the red color (Liang et al., 2019). STEVE slowly drifted equatorward (Figure 1b), and the two bands were essentially overlapped with each other at 06:37 UT (Figure 1c, at 58.2° MLAT and 22.2 hr MLT). As shown in Section 2.2, STEVE at that time was located at the magnetic zenith. The overlapping of the two arcs at the magnetic zenith indicates that the two arcs were located essentially on the same magnetic field lines with no horizontal separation. As STEVE drifted farther equatorward, the two-band structure was seen again (Figure 1d). STEVE weakened by 06:50 UT but lasted until near 07:00 UT.

The THEMIS magnetometer and imager poleward of STEVE provided a context of geomagnetic conditions in this event. The auroral onset of a large substorm occurred at 05:16 UT at ~64° MLAT (Figure 2b). The substorm

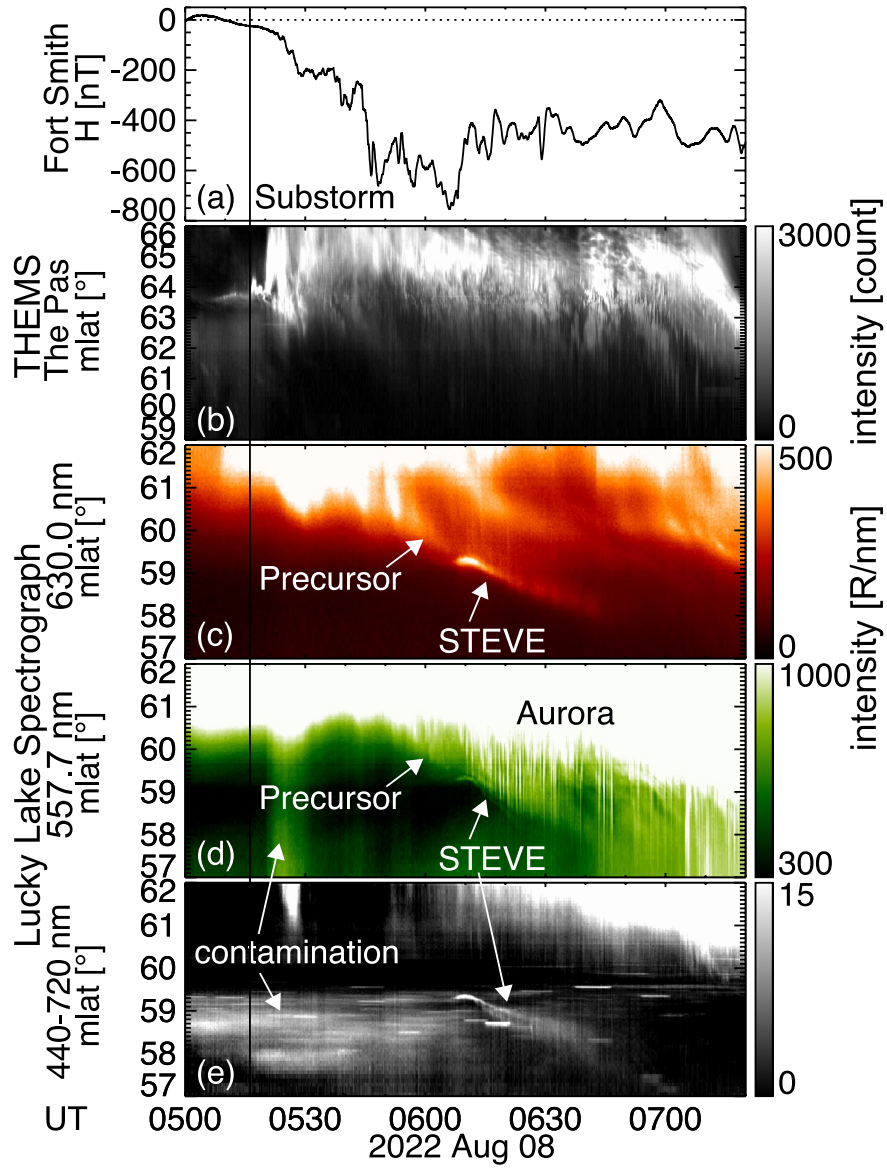

Figure 2. (a) *H*-component of ground magnetometer data at Fort Smith (67.4° MLAT and 22.2 hr MLT at 06:37 UT), (b) THEMIS ASI keogram at The Pas (63.9° MLAT and 23.1 hr MLT at 06:37 UT). TREx spectrograph data at Lucky Lake (59.2° MLAT and 22.8 hr MLT at 06:37 UT) at (c) 630.0, (d) 557.7, and (e) an average over 440–720 nm.

expansion phase lasted until 06:06 UT (Figure 2a), and thus the photographs in Figure 1 was taken during the substorm recovery phase. The spectrograph at Lucky Lake (Figures 2c–2e, 0.6 hr MLT later than Strathmore) detected a latitudinally narrow emission structure at the equatorward edge of the auroral oval during the substorm recovery phase. It has distinct continuum emissions at 440–720 nm, which are a characteristic feature of STEVE. STEVE appears to be preceded by an auroral intensification at 05:50 UT that slowly drifted equatorward. The precursor aurora is consistent with Gillies et al. (2023) and Martinis et al. (2022), but this precursor aurora involved an emission at 557.7 nm and thus is not a stable auroral red (SAR) arc. STEVE slowly drifted equatorward and was located between 58 and 59° MLAT at 06:37 UT, same latitude as the arc seen in Figure 1. The spectrograph observations confirmed that the emission of interest was located right equatorward of the auroral oval and illuminated over a broad spectral range (i.e., not proton aurora or a SAR arc but STEVE).

The DMSP 17 satellite was located in the southern hemisphere during STEVE, but its northern footprint crossed the equatorward boundary of the auroral oval, 2 hr in MLT earlier than Strathmore but simultaneous with the photograph in Figure 1d. The equatorward boundary of the electron precipitation was located around 58° MLAT

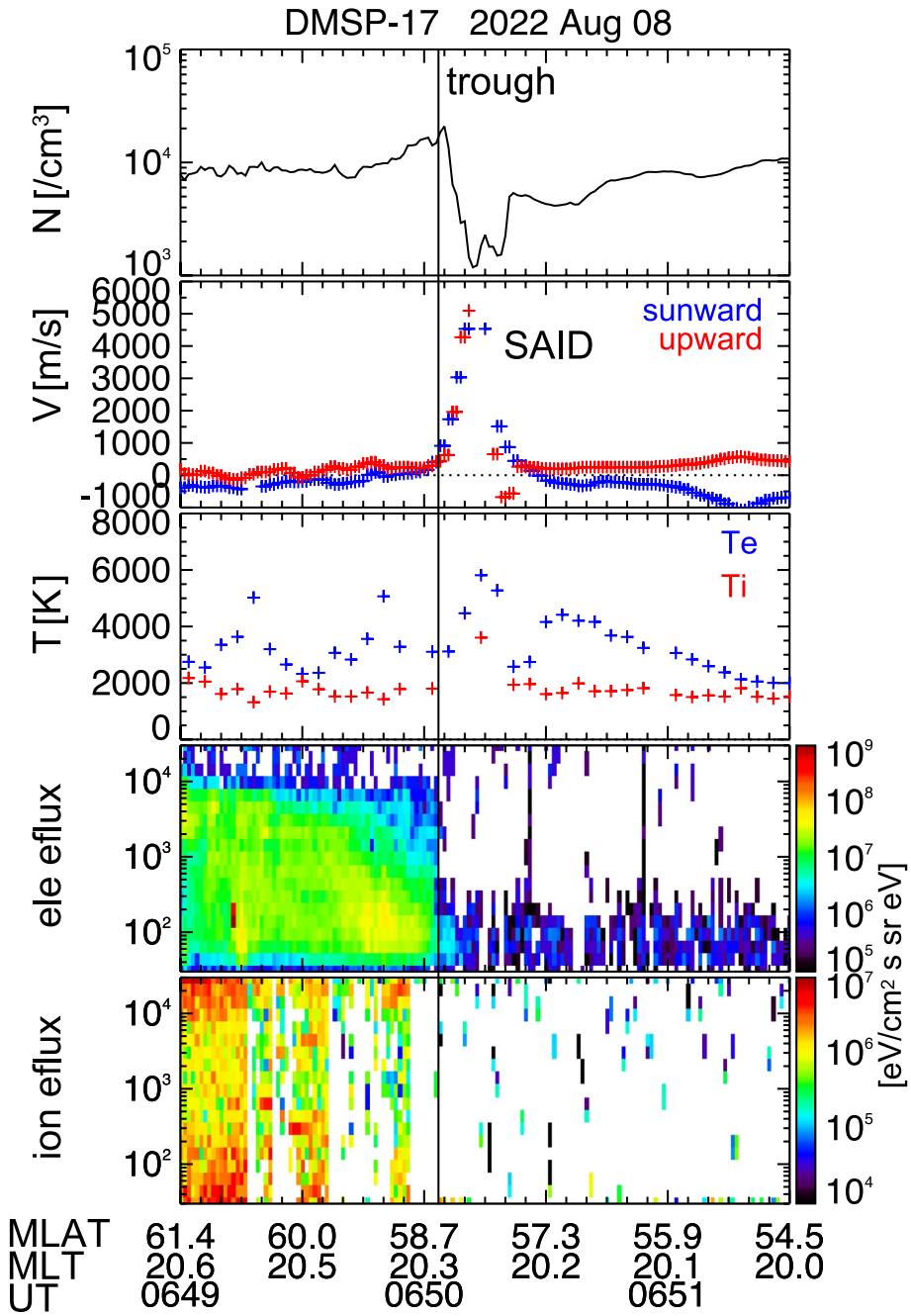

Figure 3. DMSP-17 measurements of the (a) density, (b) velocity, (c) temperature, (d) electron flux, and (e) ion flux in the southern hemisphere near the end of Strong Thermal Emission Velocity Enhancement. The labels show the latitude and local time of the satellite orbit that is mapped to the northern hemisphere.

at 06:50 UT (Figure 3d), and an intense subauroral ion drifts (SAID), density trough and elevated temperature were found just equatorward of the electron precipitation (Figures 3a–3c). These are typical ionospheric features of STEVE (Archer et al., 2019; MacDonald et al., 2018; Nishimura et al., 2019). The sunward velocity reached 4.5 km/s.

2.2. 4K High-Speed Imaging Observations

The 4K high-speed imaging of STEVE was conducted at Strathmore at 06:37–06:47 UT. A snapshot with geodetic elevation and azimuth contours is presented in Figure 4. The magnetic zenith in the International Geomagnetic

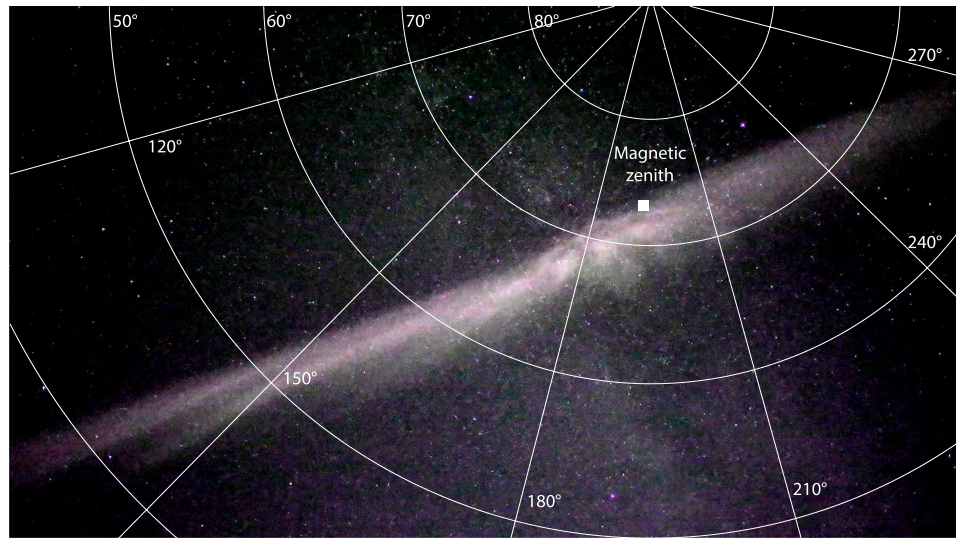

Figure 4. A snapshot of the color 4K video at 06:37:50 UT. The contour lines show the elevation and azimuth from the geographic north. The magnetic zenith is marked by the white square. The color intensity is arbitrarily scaled between 0 and 255. A sequence of images is given in Movie S1.

Reference Field model is marked by the square (73.3° inclination and 193° declination). In addition to the high resolution, another unique nature of this observation is that the STEVE arc crossed the magnetic zenith. Generally imaging observations suffer from ambiguities of horizontal and vertical structures, but structures in the present observation around the magnetic zenith can essentially be interpreted as horizontal. STEVE near the magnetic zenith of this image exhibits fine-scale structures. The remainder of this paper describes our analysis of the properties of the fine-scale structures using the 4K high-speed imaging. A sequence of images can be found in Movie S1.

Five selected snapshots around the magnetic zenith in a 1-s time interval are displayed in Figure 5. The left column shows the absolute intensity in color, and the right column shows background-subtracted images in gray-scale. Each image shows fine-scale structures within the arc. The major fine-scale structures are quasi-periodic wave-like features along the arc with a ∼10 km wavelength. The major fine-scale structures are numbered in each panel. Those structures drift westward along the arc. The arc also contained structures smaller than ∼10 km size, and they also drifted westward. More details about the scale size and drift speed are discussed below.

Figure 6 shows north-south and east-west keograms of the red, green and blue channels from the 4K images. A typical emission altitude of 200 was used to obtain the pixel positions. Here we focus on the 35 × 50 km region around the zenith so that the structures in the images can approximately be interpreted as horizontal. The quasi-periodic intensifications correspond to the fine-scale structures in Figure 5. All three color channels show essentially the same intensity variations, indicating that the fine-scale structures represent intensity variations across a broad spectral range of the STEVE emission rather than at a particular spectral line. The fine-scale structures show ∼10%–40% of intensifications above the average STEVE intensity in this time span, and thus the fine-scale structures are not small intensity fluctuations but major disturbances in the STEVE intensity.

The east-west keograms show a clear westward propagation of the fine-scale structures of STEVE. Overall, the propagation speed was constant, and the coherence of the individual fine-scale structures was maintained across the camera field of view. However, not all fine-scale structures followed the same trend. A 10-s portion of Figure 6 (Figures 7a–7c) shows that one of the fine-scale structures (highlighted by the second arrow) drifted faster and merged with the earlier fine-scale structure. It suggests that the flow field that is responsible for the westward drift of the fine-scale structures is not uniform along the arc but has small-scale structures. In another 10-s portion of the data (Figures 7d–7f), the fine-scale structure highlighted by the upward arrow faded within the field of view, while two other fine-scale structures (highlighted by the downward arrow) emerged within the field of view. Even when the fine-scale structures crossed the field-of-view, some of the fine-scale structures became brighter and dimmer during the drift. These observations suggest that the generation mechanism of the fine-scale

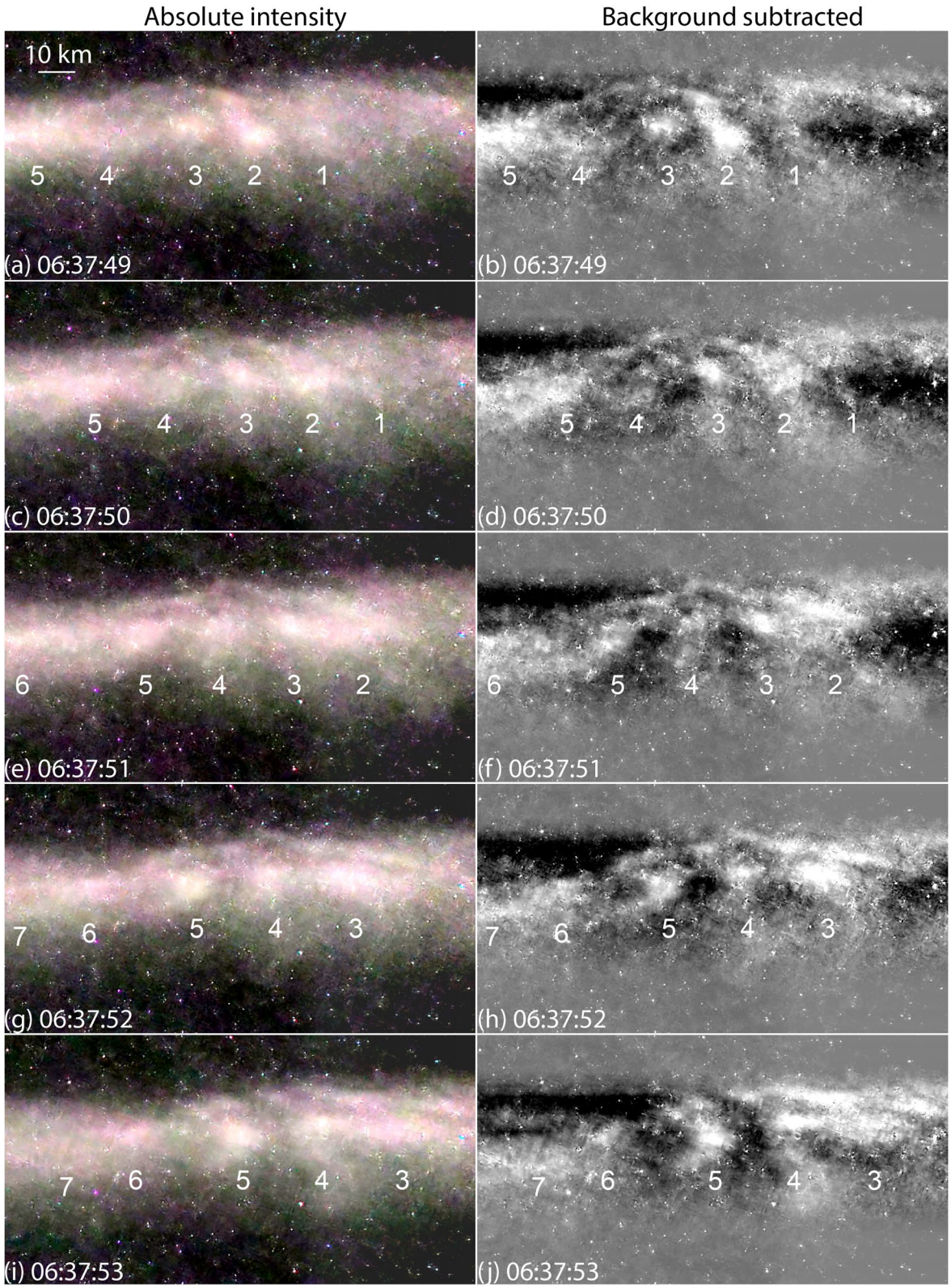

Figure 5. (Left) Selected snapshots of the 4K video after rotating the images by 22° clockwise and zooming to the region around the magnetic zenith (center of each image). A sequence of images is given in Movie S2. (Right) Same as the images on the left except that the mean intensity at each horizontal pixel lines has been subtracted and is shown in the grayscale (white being the brightest). The intensity scales are arbitrary.

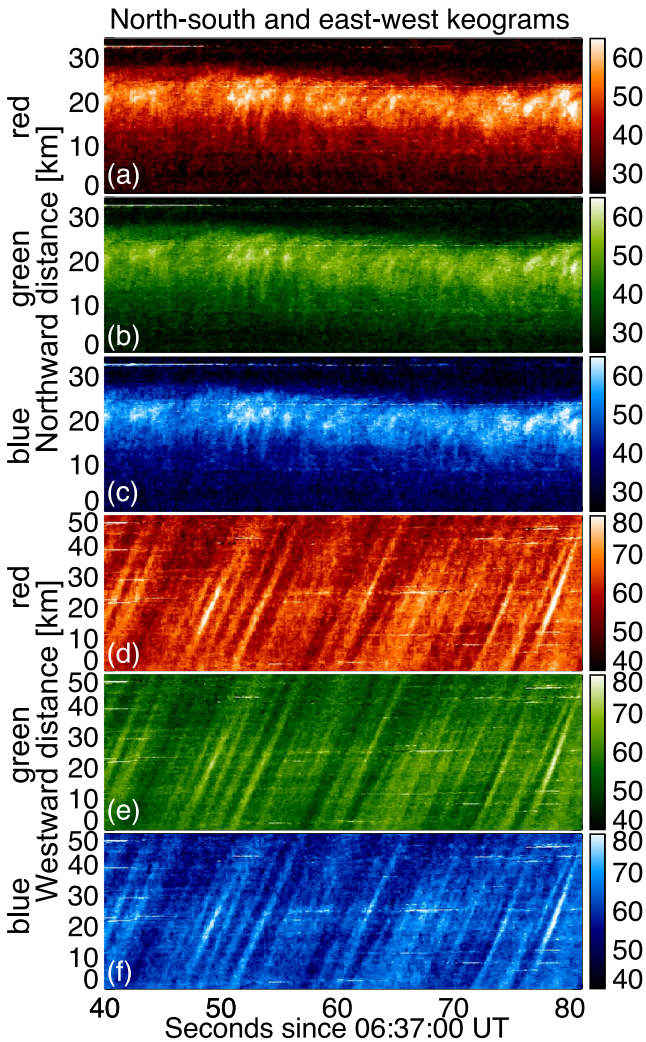

Figure 6. (a–c) North-south keograms of the red, green and blue channels from the 4K video along the meridian with the magnetic zenith. The distance is measured from 55.5° MLAT, positive northward. (d–f) East-west keograms along the Strong Thermal Emission Velocity Enhancement arc. The distance is measured from the 310.7° MLON, positive westward. The horizontal streaks are stars. The intensity is scaled to 0–255.

structures was active within the field-of-view, and that the fine-scale intensity structures could form and decay within the arc.

2.3. Properties of the Fine-Scale Structures

Figure 8a is the same as Figure 6d but presents the data over a longer (2-min) duration. The solid lines in Figure 8b traces the intensity peaks that have ≥10% intensification compared to the surrounding level. The choice of the threshold was made to identify the major fine-scale structures in Figure 8a. Fainter structures are considered in the spectral analysis below. A linear fit to each trace gave the drift speed of each fine-scale structure (Figure 8c). The average westward speed was 8.9 ± 0.7 km/s, which is comparable to the optical speed of the larger-scale structures (Gillies et al., 2020) and the intense SAID flow speed (Martinis et al., 2022; Nishimura et al., 2019). Thus we suggest that the fine-scale structures follow the ExB drift in the intense SAID flow channel. The flow speed of the intense SAID, however, is often slower (~5 km/s) (Archer et al., 2019; Nishimura et al., 2020). The DMSP observations in Figure 3 also shows a ~4.5 km/s speed. Because the DMSP observations of the SAID were away from the 4K imaging observation by ~12 min UT and 2.5 hr MLT, spatial and temporal variability of the flow speed may explain the speed difference. In addition, we should note that uncertainties of the in-situ velocity measurements for extremely fast flows have not been quantified. The true ionospheric flow speed may have substantial differences from the measured values.

While the average speed was almost constant in this time interval, the speed structure had considerable variations at short time scales. The variations suggest that the westward flow was not a uniform channel but had fine-scale structures. This is consistent with the existence of the fine-scale flow structures in subauroral polarization streams (SAPS) and SAID (Erickson et al., 2016; E. V. Mishin & Streltsov, 2023; Nishimura et al., 2022). Optical observations have an advantage of separating spatial and temporal variations compared to moving platforms. Considering that the slope of each fine-scale structure of STEVE did not change substantially but that the slopes of two adjacent fine-scale structures have differences, the flow variations are likely spatial structures that reside in the bulk SAID flow channel.

The lines in Figure 8b were used to calculate the wavelength and period of the fine-scale structures (Figures 8d and 8e). The wavelength was obtained as the vertical distance between two consecutive lines. The wave period was obtained as the horizontal distance between the two consecutive lines. Each dot in Figures 8d and 8e corresponds to these calculations for each line. The average wavelength and period were 12.4 ± 7.4 km and 1.4 ± 0.8 s. The wavelength and period had large variations at short time scales. Some fine-scale structures were very closely separated (<1 km wavelength and <0.1 s period), while others were much more separated (>25 km wavelength and 2.5 s period). The wavelength and period were highly correlated with each other, but their variations had no significant correlation with the velocity variations.

The intensity time series data near the magnetic zenith (33 km westward distance) in Figure 8a were used to obtain the power spectrum of the fine-scale structures (Figure 9). Because the fine-scale structure did not substantially change in the westward distance, the spectrum is essentially the same regardless of the choice of the westward distance. The spectrum overall follows two power laws with a spectral break at ~1 Hz. But the spectrum also has distinct peaks at >10, 4, 2, and 1.1 s (>83, 33, 16, and 9 km wavelength). Those peaks are well above the background. The last three spectral peaks seem to be in a harmonic of ~1 s, and it suggests a resonant interaction among those peaks. A factor of 2 enhancement is also seen at >5 Hz (<1.7 km wavelength).

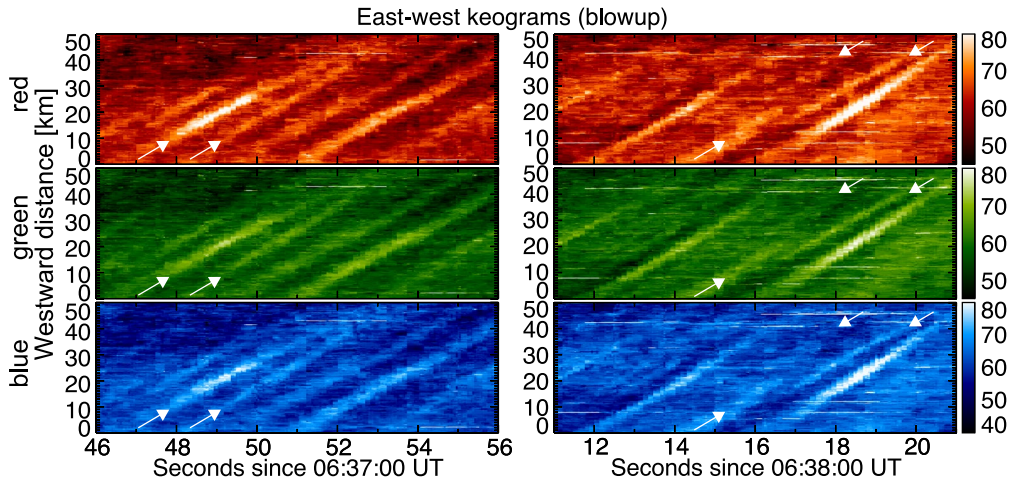

Figure 7. (a–c) Same as Figures 6d–6f but for 06:37:46–06:37:56 UT. (d–f) Same as Figures 6d–6f but for 06:38:11–06:38:21 UT.

The spectrum below 1 Hz follows a power law with a slope of −1.1. The ∼−1 spectral slope has been seen in in-situ observations of the plasma density in the subauroral ionosphere (Basu et al., 1984), although their analysis focused on smaller scales than our observations. The shear flow turbulence theory has predicted a slope of −1 below the flow shear size (Kintner & Seyler, 1985). The gradient drift instability and temperature gradient instability expect

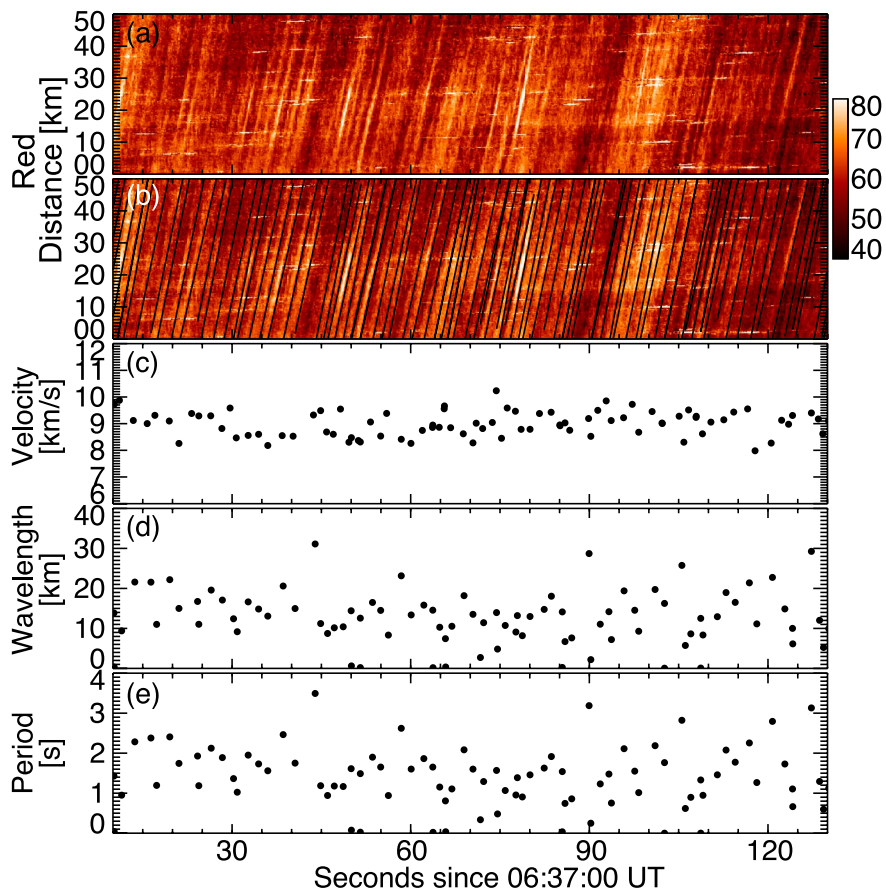

Figure 8. (a) Same as Figure 6d but for 06:37:10–06:39:10 UT. (b) Tracing of major intensity peaks (solid lines) overlaid onto the red channel keogram. (c) Westward velocity and (d) wavelength of the major fine-scale structures.

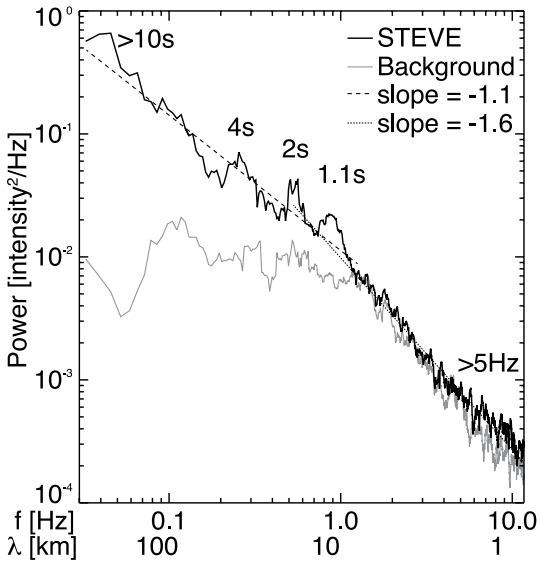

Figure 9. (Black) Power spectrum of the Strong Thermal Emission Velocity Enhancement (STEVE) intensity in the red channel in Figure 8a. (Gray) Power spectrum outside STEVE. The dashed lines show power-law fitting to the spectrum below and above 1 Hz. The wavelength is obtained by converting the period using the 8.9 km/s speed. The dashed lines are power law fitting of the spectrum.

a steeper spectrum (∼−2) (Eltrass et al., 2016; Gondarenko & Guzdar, 2004). Considering the existence of the intense SAID, the flow shear turbulence due to the intense SAID of a ∼100 km width could explain the power-law spectrum. But the presence of the spectral peaks indicates that the turbulence has not fully developed. Because the wavelength did not substantially change over time in Figure 8d, the turbulence evolves much slower than the minute time scale, or other driving mechanisms are also involved. The feedback instability simulation by E. Mishin and Streltsov (2019) predicted ∼10 km wavelength structures, and the observed wavelength is consistent with their simulation.

The spectrum above 1 Hz follows a steeper power law. A slope of −1.6 suggests the Kolmogorov turbulence with the −5/3 slope (Kolmogorov, 1991). However, this part of the spectrum is very close to the background level, and it is difficult to discuss how much this power law is related to STEVE. But as shown below, the weak enhancement above 5 Hz seems to be related to STEVE.

In order to visualize the intensity structure for the individual spectral peak, the data in Figure 6d were filtered using the cut-off periods that are labeled in Figure 10. The >5 s component corresponds to the larger-scale structures that have been studied by Gillies et al. (2020). The >5 and 2.5–5 s components highlight groups of fine-scale structures. The major fine-scale structures are seen in the 1.4–2.5 and 0.8–1.4 s components. All these components show essentially the same propagation speed, meaning that the drift velocity does not depend on the scale but follow the large-scale (likely SAID) flow speed. These components are not an artifact of the Fourier transformation but represent the major spectral peaks in Figure 9.

The 5–10 Hz component is noisy, but brief intensifications can be seen when the bright structures are seen in Figure 10a (06:37:49, 06:38:03, 06:38:13, and 06:38:19 UT). It suggests that the structures cascade to the ∼1 km scale and the small-scale structures also drift with the larger-scale structures.

3. Conclusion

We reported fine-scale STEVE structures using a 4K high-speed imaging observation, when the STEVE was located at the magnetic zenith. Although the STEVE in the all-sky photographs appeared to be a homogeneous purple/mauve arc, the high-speed imaging revealed fine-scale structures that drifted westward along the arc. Most of the fine-scale structures drifted at the same speed (8.9 ± 0.7 km/s), which agrees to the reported speed of intense SAID. The DMSP observations confirmed the existence of intense SAID during this STEVE event, although it was not simultaneous with the 4K imaging. The period and wavelength showed multiple peaks at >10, 4, 2, and 1.1 s (>83, 33, 16, and 9 km). A small enhancement in spectral power was also seen at >5 Hz (<1.7 km).

Although most of the fine-scale structures were stable during the drift across the field of view, some of the structures drifted at a different speed and merged with the adjacent structures. Some fine-scale structures also appeared and disappeared within the field of view. These features indicate that the velocity field could have fine-scale perturbations, and the fine-scale intensity structures could form and decay within the STEVE arc.

The present study showed that the perception of the homogeneous arc (Størmer, 1935) does not represent the true character of STEVE. STEVE consists of multi-scale structures down to the ∼10 and ∼1 km size, and thus large-scale observations and modeling may not fully answer how STEVE forms. A major challenge is how the ionosphere and thermosphere create such fine-scale structures. If the NO_2 continuum through the $NO + O \rightarrow NO_2 + h\nu$ chemical reaction is responsible for the STEVE emission (Gillies et al., 2019; Harding et al., 2020; Mende et al., 2019), the long chemical lifetime (hours to days) of NO (Barth et al., 2001; Gattinger et al., 2010) would not explain any fine-scale structures. The emission lifetime should be within seconds to explain the observed fine-scale structures. Vibrational and electronical excitation of N_2 has a relaxation time scale of the order of a minute (E. Mishin et al., 2000; E. Mishin & Streltsov, 2019). Although it is still longer than the observational expectation, it

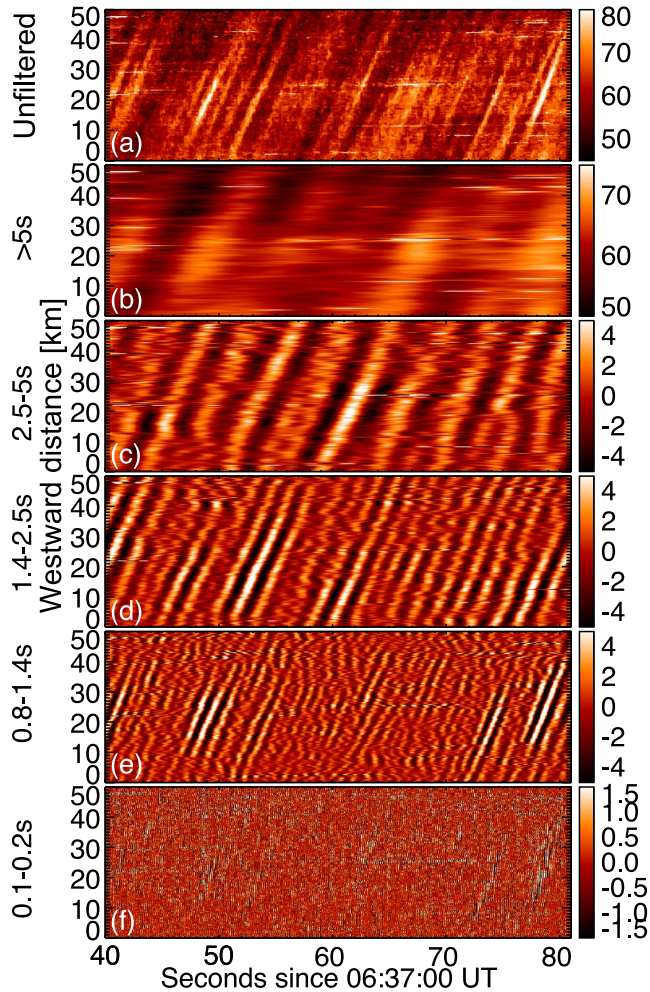

Figure 10. (a) Same as Figure 6d. The subsequent panels show data filtered at (b) >5, (c) 2.5–5, (d) 1.4–2.5, (e) 0.8–1.4, and (f) 0.1–0.2 s.

provides a more realistic emission time scale. In addition, since it is unlikely that the neutral species move at the speed of the fine-scale structures, the plasma density that drifts at the SAID velocity and interacts with neutrals should be highly structured. SAID flow channel and the ionospheric trough density gradients could be unstable and cascade to smaller scales through turbulence. Numerical simulations are required to investigate how density structures evolve under STEVE-like conditions.

Data Availability Statement

The citizen scientist data are available at Amazing Sky (Dyer, 2022). The TREx spectrograph and THEMIS ASI and ground magnetometer data were obtained Angelopoulos (2007) and Donovan (2017).

References

Angelopoulos, V. (2007). THEMIS ASI and ground magnetometer data [Dataset]. University of California. Retrieved from http://themis.ssl.berkeley.edu/themisdata/thg/l1/asi/

Archer, W. E., Gallardo-Lacourt, B., Perry, G. W., St.-Maurice, J.-P., Buchert, S. C., & Donovan, E. F. (2019). Steve: The optical signature of intense subauroral ion drifts. *Geophysical Research Letters*, *46*(12), 6279–6286. https://doi.org/10.1029/2019gl082687

Barth, C. A., Baker, D. N., Mankoff, K. D., & Bailey, S. M. (2001). The northern auroral region as observed in nitric oxide. *Geophysical Research Letters*, *28*(8), 1463–1466. https://doi.org/10.1029/2000gl012649

Basu, S., Basu, S., MacKenzie, E., Coley, W. R., Hanson, W. B., & Lin, C. S. (1984). F region electron density irregularity spectra near auroral acceleration and shear regions. *Journal of Geophysical Research*, *89*(A7), 5554–5564. https://doi.org/10.1029/JA089iA07p05554

Acknowledgments
This work was supported by NASA Grants 80NSSC18K0657, 80NSSC20K0725, 80NSSC21K1321, 80NSSC22K0323, 80NSSC22K0749, 80NSSC22M0104, and 80NSSC23K0410, NSF Grants AGS-1907698 and AGS-2100975, and AFOSR Grants FA9550-23-1-0634 and FA9550-23-1-0614. THEMIS is supported by NASA NAS5-02099 and Canada Foundation for Innovation. We thank ISSI Bern/ISSJ-BJ for the "Multi-Scale Magnetosphere-Ionosphere-Thermosphere Interaction" (project #511), "Magnetotail Dipolarizations: Archimedes Force or Ideal Collapse?", and "Auroral Research Coordination: Towards Internationalised Citizen Science (ARCTICS)" teams.

Donovan, E. (2017). TREx spectrograph data [Dataset]. University of Calgary. Retrieved from https://data.phys.ucalgary.ca/sort_by_project/TREx/spectrograph/

Dyer, A. (2022). Citizen scientist image data [Dataset]. Amazing Sky. Retrieved from https://amazingsky.net/2022/08/

Eltrass, A., Scales, W. A., Erickson, P. J., Ruohoniemi, J. M., & Baker, J. B. H. (2016). Investigation of the role of plasma wave cascading processes in the formation of midlatitude irregularities utilizing GPS and radar observations. *Radio Science*, *51*(6), 836–851. https://doi.org/10.1002/2015RS005790

Erickson, P. J., Matsui, H., Foster, J. C., Torbert, R. B., Ergun, R. E., Khotyaintsev, Y. V., et al. (2016). Multipoint MMS observations of fine-scale SAPS structure in the inner magnetosphere. *Geophysical Research Letters*, *43*(14), 7294–7300. https://doi.org/10.1002/2016GL069174

Gattinger, R. L., McDade, I. C., Alfaro Suzán, A. L., Boone, C. D., Walker, K. A., Bernath, P. F., et al. (2010). NO_2 air afterglow and O and NO densities from Odin-OSIRIS night and ACE-FTS sunset observations in the Antarctic MLT region. *Journal of Geophysical Research*, *115*(D12), D12301. https://doi.org/10.1029/2009JD013205

Gillies, D. M., Donovan, E., Hampton, D., Liang, J., Connors, M., Nishimura, Y., et al. (2019). First observations from the TREx spectrograph: The optical spectrum of STEVE and the picket fence phenomena. *Geophysical Research Letters*, *46*(13), 7207–7213. https://doi.org/10.1029/2019gl083272

Gillies, D. M., Liang, J., Donovan, E., & Spanswick, E. (2020). The apparent motion of STEVE and the picket fence phenomena. *Geophysical Research Letters*, *47*(20), e2020GL088980. https://doi.org/10.1029/2020gl088980

Gillies, D. M., Liang, J., Gallardo-Lacourt, B., & Donovan, E. (2023). New insight into the transition from a SAR arc to STEVE. *Geophysical Research Letters*, *50*(6), e2022GL101205. https://doi.org/10.1029/2022gl101205

Gondarenko, N. A., & Guzdar, P. N. (2004). Density and electric field fluctuations associated with the gradient drift instability in the high-latitude ionosphere. *Geophysical Research Letters*, *31*(11), L11802. https://doi.org/10.1029/2004GL019703

Harding, B. J., Mende, S. B., Triplett, C. C., & Wu, Y.-J. J. (2020). A mechanism for the STEVE continuum emission. *Geophysical Research Letters*, *47*(7), e2020GL087102. https://doi.org/10.1029/2020gl087102

Kintner, P. M., & Seyler, C. E. (1985). The status of observations and theory of high latitude ionospheric and magnetospheric plasma turbulence. *Space Science Reviews*, *41*(1–2), 91–129. https://doi.org/10.1007/bf00241347

Kolmogorov, A. (1991). The local structure of turbulence in incompressible viscous fluid for very large Reynolds numbers. *Proceedings of the Royal Society of London. Series A*, *434*, 9–13. https://doi.org/10.1098/rspa.1991.0075

Liang, J., Donovan, E., Connors, M., Gillies, D., St-Maurice, J. P., Jackel, B., et al. (2019). Optical spectra and emission altitudes of double-layer STEVE: A case study. *Geophysical Research Letters*, *46*(23), 13630–13639. https://doi.org/10.1029/2019gl085639

MacDonald, E. A., Donovan, E. F., Nishimura, Y., Case, N. A., Gillies, D. M., Gallardo-Lacourt, B., et al. (2018). New science in plain sight: Citizen scientists lead to discovery of optical structure in the upper atmosphere. *Science Advances*, *4*(3), eaaq0030. https://doi.org/10.1126/sciadv.aaq0030

Martinis, C., Griffin, I., Gallardo-Lacourt, B., Wroten, J., Nishimura, Y., Baumgardner, J., & Knudsen, D. J. (2022). Rainbow of the night: First direct observation of a SAR arc evolving into STEVE. *Geophysical Research Letters*, *49*(11), e2022GL098511. https://doi.org/10.1029/2022gl098511

Mende, S. B., Harding, B. J., & Turner, C. (2019). Subauroral green STEVE arcs: Evidence for low-energy excitation. *Geophysical Research Letters*, *46*(24), 14256–14262. https://doi.org/10.1029/2019gl086145

Mishin, E., Carlson, H. C., & Hagfors, T. (2000). On the electron distribution function in the F region and airglow enhancements during HF modification experiments. *Geophysical Research Letters*, *27*(18), 2857–2860. https://doi.org/10.1029/2000GL000075

Mishin, E., & Streltsov, A. (2019). STEVE and the picket fence: Evidence of feedback-unstable magnetosphere-ionosphere interaction. *Geophysical Research Letters*, *46*(24), 14247–14255. https://doi.org/10.1029/2019gl085446

Mishin, E. V., & Streltsov, A. V. (2023). The inner structure of STEVE-linked SAID. *Geophysical Research Letters*, *50*(8), e2023GL102956. https://doi.org/10.1029/2023gl102956

Nishimura, Y., Donovan, E. F., Angelopoulos, V., & Nishitani, N. (2020). Dynamics of auroral precipitation boundaries associated with STEVE and SAID. *Journal of Geophysical Research: Space Physics*, *125*(8), e2020JA028067. https://doi.org/10.1029/2020ja028067

Nishimura, Y., Dyer, A., Kangas, L., Donovan, E., & Angelopoulos, V. (2023). Unsolved problems in Strong Thermal Emission Velocity Enhancement (STEVE) and picket fence. *Frontiers in Astronomy and Space Sciences*, *10*, 01–09. https://doi.org/10.3389/fspas.2023.1087974

Nishimura, Y., Gallardo-Lacourt, B., Zou, Y., Mishin, E., Knudsen, D. J., Donovan, E. F., et al. (2019). Magnetospheric signatures of STEVE: Implications for the magnetospheric energy source and interhemispheric conjugacy. *Geophysical Research Letters*, *46*(11), 5637–5644. https://doi.org/10.1029/2019gl082460

Nishimura, Y., Goldstein, J., Martinis, C., Ma, Q., Li, W., Zhang, S. R., et al. (2022). Multi-scale density structures in the plasmaspheric plume during a geomagnetic storm. *Journal of Geophysical Research: Space Physics*, *127*(3), e2021JA030230. https://doi.org/10.1029/2021ja030230

Parnikov, S. G., Ievenko, I. B., & Koltovskoi, I. I. (2022). Subauroral luminosity STEVE over Yakutia during a substorm: Analysis of the event of March 1, 2017. *Geomagnetism and Aeronomy*, *62*(4), 434–443. https://doi.org/10.1134/s0016793222030136

Størmer, C. (1935). Remarkable aurora-forms from southern Norway. I, Feeble homogeneous arcs of great altitude. *Geofysiske Publiskasjoner*, *11*(5), 3–19.

Wilson, W. E. (1891). A rare phenomenon. *Nature*, *44*(1143), 494. https://doi.org/10.1038/044494c0